

Supplementary Appendix

This appendix has been provided by the authors to give readers additional information about their work.

Supplement to: Kim J, Hu C, Moufawad El Achkar C, et al. Patient-customized oligonucleotide therapy for a rare genetic disease. *N Engl J Med* 2019;381:1644-52. DOI: 10.1056/NEJMoa1813279

Supplementary Appendix
for
Patient-customized Oligonucleotide Therapy for a Rare Genetic Disease
by Kim, Hu, et al.

TABLE OF CONTENTS

SUPPLEMENTARY METHODS	2
SUPPLEMENTARY TEXT	11
SUPPLEMENTARY FIGURES S1–S18	17
SUPPLEMENTARY TABLES S1–S6	35
REFERENCES.....	40

SUPPLEMENTARY METHODS

Human subjects

Genomic and functional studies for the patient and family members were performed after obtaining appropriate consent under an institutional review board (IRB)-approved protocol at Boston Children's Hospital. Separate written informed parental consent was obtained for an expanded access treatment trial with milasen, after the IRB approval of the clinical protocol. In detail, the clinical protocol was initially for one year, but can be stopped or extended based on the clinical outcome and parental requests. The goal of the treatment, as explained and consented to by the parents, was to preserve the patient's quality of life; both parents understood that the investigational therapy cannot reverse the damage that has already occurred. It was also explained and understood that while treatment might in theory improve the function of damaged but not yet irreversibly injured cells, there was no way to know for sure if such cells existed in appreciable quantities, and/or whether such impact would manifest in clinical benefit. Annual renewal of this compassionate use protocol is subject to review by the medical team, with input from the family, to ensure that the goal is being met. Formally, the final decision to continue or stop treatment was explicitly placed in a clinician, who is not the scientific principal investigator of this study. This structure was chosen to separate scientific and clinical responsibilities.

Whole genome sequencing (WGS) and Sanger sequencing

Genomic DNA was isolated from blood samples of the patient's trio. WGS library preparation and sequencing runs were performed by Claritas Genomics and WuXi NextCODE using Illumina HiSeq X Ten. Reads were aligned to GRCh37/hg19 using BWA.¹ QC and variant calling were performed based on the GATK best practice guidelines.² WGS-identified mutations were validated by Sanger sequencing at an independent CLIA facility (Claritas Genomics). The full SVA sequence was identified by primer walking PCR and Sanger sequencing. Primer sequences are provided in **Figure S3B**.

Algorithmic detection of transposable elements

In order to systematically identify transposable element (TE) insertions as potential pathogenic variants, we analyzed WGS data from the trio using memTea, a revised version of Tea³ to support BWA mem alignment. Briefly, the memTea method detects a TE insertion by looking for clusters of two types of sequencing reads near insertion breakpoints: 1) repeat-anchored mate (RAM) reads that uniquely map to the reference genome but have their paired mate reads mapping to our custom TE sequence library, and 2) clipped reads that span insertion breakpoints and therefore only map partially to the reference genome, with unmapped (*i.e.*, clipped) subsequences originating from an inserted TE. A pileup of clipped reads allows us to pinpoint insertion breakpoints at single-nucleotide resolution and extract signatures such as the polyA tail and target site duplication, which are hallmarks of target-primed reverse transcription (TPRT)-mediated retrotransposition. Using a parameter set that requires a minimum of 3 RAMs and 2 clipped reads (“--mem --ram_cutoff 3 --oneside_ram --min_acr 2 --include_head_clip”), we identified the SVA insertion in the genomes of both the patient and the mother with the mechanistic features of TPRT including the polyA tail and 14 bp target site duplication. To assess the frequency of the patient’s SVA retrotransposon in human population, WGS data from over 800 individuals (282 TCGA cancer patients, 20 patients in an unrelated cohort of individuals with Autism Spectrum Disorder (ASD), and 500 unaffected parents from the Simons Simplex Collection for ASD) were analyzed based on Tea.⁴

Skin fibroblast and lymphoblastoid cell line

Fibroblast: Patient’s skin fibroblasts were derived from 3 mm skin punch biopsy and explant culture. The fibroblasts were maintained and passaged in media containing Alpha MEM (Irvine Scientific) and Chang Medium B (Irvine Scientific), supplemented with Chang C Supplement (Irvine Scientific), GlutaMAX (Life Technologies), and 10% FBS. Fibroblasts only under passage 20 were used for experiments.

Lymphoblastoid Cell Line (LCL): From each family member of the patient (patient, mother, father, brother), 5 ml of peripheral blood was drawn into a heparinized blood tube. Mononuclear cells were isolated by density gradient centrifugation using Ficoll Histopaque-1077 (Sigma-Aldrich). LCLs were established by infecting the mononuclear cells with Epstein-Barr virus and culturing for 2–4 weeks in RPMI-1640 medium supplemented with 10% FBS.

RNA sequencing (RNA-seq)

For RNA-seq of the fibroblasts (**Fig. 2C**), total RNA was isolated using a standard column-based procedure. RNA-seq libraries were prepared using WaferGen PrepX kit (WaferGen Biosystems). Sequencing was performed on an Illumina NextSeq machine using 2×150 bp paired-end reads. We repeated library preparation and sequencing four more times using alternative kits, KAPA Hyper Prep kit (KAPA Biosystems; for library preparation) and HiSeq 2500 (for sequencing; 2×100 bp). As the replicates showed consistent results, we aggregated the data from all runs. For quality control of sequencing reads, we used Cutadapt (version 1.11) and Trimmomatic (version 0.36)⁵ to trim adapter sequences and low quality bases at the ends. Reads that were trimmed to be shorter than 30 nt were removed. Reads that contain a region of consecutive low quality bases in the middle were also removed. For alignment, HISAT2 (version 2.1.0) was used to map reads on human genome (GRCh37/hg19) in the paired-end, two-pass mode, generating alignments in SAM format. Alignment by an alternative algorithm (STAR, version 2.5.4) also produced a consistent result. Using Samtools, the SAM files were converted to BAM format and subsequently sorted and indexed by chromosomal coordinate. Gene annotation was not provided to the alignment program in order to avoid any biased alignment favoring annotated splice junctions. The sorted BAM files were indexed using Samtools. IGV was used to draw Sashimi plots, which showed the number of reads supporting splice junctions in the genomic region containing *MFSD8/CLN7* exon 5 through 7. Similar experimental methods and analysis algorithms were applied for the RNA-seq of the lymphoblastoid cell lines derived from the patient's family members (**Fig. S5A**).

Reverse transcriptase PCR (RT-PCR) validation of missplicing

Total RNA was isolated from each patient family member's blood and LCLs. cDNA was synthesized using the standard reverse transcription procedure with the oligo-dT primer. For PCR, primers F_e5-6 (5'-TGGAGCAGGAAATGTAGCAGTT), R_e7 (5'-TGTTAGTGCTTGTTGAGGGCT), and R_i6 (5'-ATTCCCAGGAAGGCGCTAAG) were used. F_e5-6 and R_e7 primers yield a 233 bp product representing the wild type splicing connecting exons 6 and exon 7, and F_e5-6 and R_i6 primers yield a 190 bp product representing the abnormal splicing connecting exon 6 and the cryptic splice site in intron 6 (**Fig. S5B**).

Antisense oligonucleotide (ASO) screening by multiplex PCR

Patient's fibroblasts were transfected with ASOs using Lipofectamin 3000 (ThermoFisher). Research-grade (standard desalted) ASOs were custom-manufactured at IDT and Microsynth. ASO sequences and chemistries are provided in **Table S1**. Transfected cells were harvested at 24 hours. Total RNA and cDNA was prepared using the standard procedure. For PCR, the same primers used in the standard RT-PCR (**Fig. S5B**), F_e5-6, R_i6, and R_e7, were used, except for that all three primers were used in the same multiple PCR reaction yielding two PCR products with size 190 bp (representing abnormal splicing) and 233 bp (representing wild type splicing; **Fig. S6**). Quantities of the wild type and abnormal splicing were measured by quantifying the band intensity on agarose gels (**Fig. 2B**).

ASO validation by quantitative PCR

For dose-response (**Fig. S8**), fibroblasts were electroporated with ASOs by using the Neon Transfection System (ThermoFisher). ASO concentrations ranged from 0–500 nM, calculated on a fully medium-diluted basis. Cells were harvested 24 hours after electroporation. For blinded replication experiments by an independent laboratory (**Fig. S7**), both fibroblasts and LCLs were transfected with ASOs at 100 nM concentration by a standard lipid-based procedure. Total RNA was prepared using a standard column-based procedure. Reverse transcription and qPCR was conducted in one step by using qScript XLT One-

Step RT-qPCR ToughMix, Low ROX kits (VWR Quanta Biosciences). Three sets of primers and probes were used for amplification of two splice isoforms of *MFSD8/CLN7* (E6-E7 and E6-i6) as well as *GAPDH* loading control. The primer and probe sequences are provided in **Table S2**.

Prediction of off-target binding

Progressively end-trimmed versions of milasen and nusinersen sequences, as well as sequences in 1 or 2 substitutions away from each sequence, were generated. STAR (version 2.5.4; with the default parameters)⁶ was used to align the generated sequences on the human genome GRCh37/hg19 assembly. Alignment results were analyzed with respect to the RefSeq gene annotation.

Electron microscopy

Patient and control fibroblasts (*MFSD8/CLN7* wild type human foreskin fibroblasts; BJ cell line) were plated on 35 mm culture dishes, and the patient fibroblasts were transfected with 100 nM milasen or a scrambled oligonucleotide. Four days post-transfection, the cells were fixed in 2.5% glutaraldehyde/PBS for 30 minutes and then washed with PBS (6X, 5 minutes each). After fixation with 1% OsO₄/PBS for 1 hour, the samples were dehydrated with 50% ethanol (2X, 5 minutes each) and then 70% ethanol (2X, 10 minutes each). Next, the samples were stained with 1% uranyl acetate in 70% ethanol for 45 minutes, and further dehydrated using 90% ethanol (2X, 10 minutes each) and 100% ethanol (3X, 10 minutes each). To evaporate the ethanol, 1:1 EMbed resin mix (EMbed 812, DDSA, NMA) in 100% ethanol was added to the samples for 1 hour with the lid off. Next, EMbed resin mix alone was added for 1 hour, followed by final embedding with EMbed resin mix + DMP30 overnight at 60°C. The embedded samples were pried from the dishes, cut and placed on beam embedding capsules. The samples were sectioned on an ultramicrotome and viewed on an FEI Tecnai Spirit G2 TEM operated at 80 kV. Images were examined in a blinded manner and storage level was scored according to the abundance of vacuoles observed per cell. Scoring was performed on a scale of 0 to 5, with 0 representing the lowest and 5 representing the highest amount of vacuole accumulation. Control wild-type fibroblasts defined a 0 score, whereas

MFSD8/CLN7 mutant fibroblasts that contained storage in >50% of the cytoplasm represented the maximum score of 5. All imaging work was performed at the Northwestern University Center for Advanced Microscopy.

Lysosomal function assays

The patient's fibroblasts and control fibroblasts (BJ cell line) were transfected with a scrambled oligonucleotide or milasen at 100 nM by a standard lipid-based transfection. Cells were prepared for assays at 48 hours post transfection. Lysosomal and cytosolic activity of lysosomal beta-Glucocerebrosidase (GCase) was measured in living cultures of patient and control fibroblasts using the artificial GCase substrate, PFB-FD-Gluc. The measured activity was normalized to lysosomal mass, which is quantified by cascade blue dextran, and analyzed as previously described.⁷ Autofluorescent pigment was measured by quantifying fluorescence of living cells cultured in phenol red-free media (excitation at 485 nm, emission at 530 nm) on a microplate reader. For autophagic flux assays, fibroblasts were treated with either DMSO (vehicle control) or bafilomycin A1 (baf A1; 200 nM, 2 hours) to evaluate autophagosome-lysosome fusion. Cells were extracted in 1% Triton X-100 buffer and the response to baf A1 was analyzed by western blot analysis for LC3-II levels. α -tubulin (α -tub) or GAPDH levels were also probed as loading controls. For quantification of the autophagic flux, the intensity of LC3-II band was normalized by that of GAPDH band.

Manufacturing and formulation of milasen

Milasen was manufactured by TriLink and formulated by Brammer Bio as 2 mL 8.5 mg/mL solution in artificial CSF (Elliotts B). As quality control, multiple release tests were performed, which includes but not limited to tests for appearance (clear solution, free from visible particles), identity (within 5% of expected mass of 8829.5 amu), purity (determined as 98.2% pure by HPLC), pH (7.46), bioburden (<1 CFU/10 mL), bacterial endotoxins (<0.5 EU/mL), and sterility (no growth).

Animal toxicology

Animal toxicology studies were conducted at Charles River Laboratories following GLP requirements. Milasen was administered by intrathecal bolus injection via a catheter implanted at the lumbar level to female Sprague Dawley rats. Endpoints evaluated in this study included clinical signs (such as posture, tonic spasms, alertness, and gait), body weights, food consumption, behavioral neurological examination/functional observation battery (FOB), clinical pathology (hematology, biochemistry, coagulation and urinalysis parameters), gross observations at necropsy, organ weights, and histopathology.

Clinical study design

Diet and confounding factors: Diet and medication regimen adherence (topiramate, 72 mg b.i.d.) were logged in a parent-maintained patient diary and remained consistent throughout the period of the study.

Drug administration: In this open-label, escalating dose study, the study subject received milasen every two weeks, with doses of 3.5, 7, 14, 21, 28, 35, and 42 mg. This was followed by two more loading doses of 42 mg every two to three weeks, and tenth and eleventh doses of 42 mg every three months (**Fig. 3A** and **S14A**). At each dose, milasen diluted in 5 mL of Elliotts B solution was administered by intrathecal bolus via lumbar puncture under monitored anesthesia care in an operative suite. The patient underwent 48 hours of inpatient observation after each dose up to the third 42 mg dose; for subsequent doses, she was observed in a post anesthesia care unit for four hours prior to discharge to home.

Safety: Safety assessments included documentation of adverse events (AEs), vital sign checks, physical/neurologic examinations, clinical laboratory tests (complete blood counts, serum chemistries, coagulation time, liver function tests, creatine kinase levels, urinalysis, as well as CSF cell count, total protein, and glucose), and ECGs at each dose, as well as screening for motor or sensory impairments before and after each intrathecal dosing.

Motor impairment test: The modified Bromage scale,^{8,9} widely used in studies of regional anesthesia in both adults and children,^{10,11} was used to assess motor function in the hours immediately following each dose administration. Bromage scores were recorded at baseline prior to lumbar puncture and at 3, 6, 12 and 24 hours post lumbar puncture. If 24 hour scores showed no impairment compared to baseline, then no additional testing was performed. If 24 hour scores showed continued impairment, then scores were repeated every 24 hours until they returned to baseline.

Sensory threshold test: To monitor for possible transient lower extremity sensory impairments in the hours immediately following each dose administration, von Frey filaments were applied to the plantar surface of the foot in ascending order of increasing intensity (starting with the smallest first) to determine mechanical thresholds for evoking either a flinch, withdrawal, or a facial expression response. Each filament was applied three times and the behavioral response was recorded. The sensory threshold was defined as the vFh (g-force) required to evoke three responses. The inter-stimulus interval between each stimulus was approximately 2 seconds. A pin prick method was used when no response was present to the von Frey filament stimulation.

Pharmacokinetic (PK) profiling: Blood and CSF samples were drawn for PK assessments. CSF samples were withdrawn immediately prior to each dose administration. Also, at each dose, blood samples were drawn pre-dosing, immediately post dose, and at 1, 2, 4, 6, 8, 12, 16, and 24 hours post-dosing. A nuclease-dependent hybridization ELISA was used for sensitive determination of oligonucleotide concentration. The assay was calibrated and performed at Charles River Laboratories. The bioanalytical method utilized a surface-anchored oligonucleotide probe (“cutting probe”), with full complementarity to the milasen sequence, that is highly specific for full-length drug, owing to treatment with a single-strand specific nuclease to cleave any un-hybridized probe or exposed single-stranded material. The analysis was performed in compliance with the OECD Principles of GLP.

Clinical outcome measures: Exploratory clinical assessments include seizure frequency and duration (parent-recorded seizure diaries and periodic overnight EEGs), neuropsychology evaluations (selected items from the Bayley Scales of Infant and Toddler Development, and the Vineland Adaptive Behavior Scale), motor function evaluation (according to GMFM-88 scoring system), neurologic examinations, and MRI/MRS of the head.

SUPPLEMENTARY TEXT

WGS variant interpretation

Analyses of the WGS data, initially focusing on the *MFSD8/CLN7* locus, demonstrated that the proband bore a total of 16 non-reference single nucleotide variants (SNVs). Among these was the previously described heterozygous c.1102G>C mutation, which was demonstrated to be paternally inherited. We therefore searched for the presence of an additional maternally inherited mutation in *MFSD8/CLN7*. However, none of the remaining 15 SNVs in the *MFSD8/CLN7* locus were consistent with inactivating function. All were noncoding (*e.g.*, intronic or in UTRs), and 14/15 had allele frequencies consistent with common polymorphisms (ExAC or dbSNP allele frequency > 1%). The 15th was a single base substitution (chr4:128874711T>G, GRCh37/hg19) deep in intron 3 (3 kb away from the nearest exon), in the midst of a 28 bp long homopolymer T stretch, which is highly unlikely to impact splicing. Careful examination of read depth over the *MFSD8/CLN7* also failed to demonstrate any evidence of copy number alteration. No likely pathogenic mutations were found in any of the other 13 genes associated with Batten disease.

Prediction of off-targets

Since off-target binding of an oligonucleotide can lead to side effects and toxicity, we examined potential off-target binding sites of milasen in the human genome. To simulate binding of end-degraded oligonucleotide products or partial binding of an intact oligonucleotide with nucleotide mismatches at either end, we conducted computational sequence alignments to map progressively smaller subsequences of milasen to the human reference genome sequence (**Fig. S9A**). Milasen did not have any off-target matches to the genome until it was trimmed down by 6 nucleotides (16mer). In comparison, nusinersen had off-target matches when trimmed down by only 1 nucleotide (17mer; **Fig. S9B**). This analysis suggested that milasen is likely to have a comparable or smaller off-target binding footprint on the human genome than nusinersen. We confirmed that the none of the 16mer predicted off-targets of milasen is

antisense (thus, able to bind) to critical functional regions (exonic or <0.5kb from the closest splice junction) of annotated human mRNAs. Furthermore, we also confirmed that even when allowing up to two internal mismatches, milasen does not have any match in the reference human genome.

Lysosomal function

We asked whether milasen/TY777 would restore lysosomal function in our patient's fibroblasts.

Fibroblasts from the proband exhibited several cellular phenotypes characteristic of lysosomal dysfunction (**Fig. S11A**). On electron microscopy, our patient's fibroblasts showed increased numbers and sizes of intracellular vacuoles (**Figs. 2D** and **S10**) whereas *MFSD8/CLN7* wild-type control fibroblasts did not. This increase represents an accumulation of storage material in the cells of Batten disease patients.¹² When the patient fibroblasts were treated with milasen/TY777, the number and size of vacuoles were significantly reduced compared to fibroblasts treated with a scrambled oligonucleotide. Furthermore, a biochemical assay measuring lysosomal mass (by measuring pH of acidic organelles, *i.e.*, lysosomes) showed the total lysosomal mass in patient fibroblasts to be twice that of control fibroblasts (**Fig. 11B**), consistent with the increase in lysosomal number and size seen in many lysosomal storage disease states.¹³ Patient fibroblasts also demonstrated a strong autofluorescence signal not seen in controls, a well-documented observation in Batten disease that correlates with the lysosomal accumulation of lipid and protein aggregates. In addition, patient fibroblasts possessed ~50% reduced enzymatic hydrolase activity within lysosomes, but a ~2X increased activity within the cytosol (*i.e.*, outside of lysosomes), indicating a breakdown of proper compartmentalization of lysosomal enzyme activity. Lastly, patient fibroblasts showed reduced autophagic flux (**Figs. S11B** and **S12A**), mirroring observations in *MFSD8/CLN7* knock-out mice.¹⁴

Milasen-transfected patient fibroblasts showed substantial reduction of lysosomal mass, reduction of accumulation of autofluorescence pigment, increases in hydrolase activity within lysosomes, reduction in hydrolase activity outside of lysosomes, and restoration of autophagic flux, compared to controls transfected with a scrambled oligonucleotide (**Figs. S11C** and **S12A**). In addition, the hydrolase activity

within lysosomes was increased in a dose-dependent manner by milasen, but not by a scrambled oligonucleotide (**Fig. S12B**). Together, these results provided evidence that oligonucleotide treatment can not only reverse abnormal splicing but also restore cellular lysosomal function.

Rat toxicology

Single-dose tolerability: Rats were given a single intrathecal injection of milasen diluted in 50 μ l artificial CSF (Elliotts B). Animals were divided into four groups by dose level (20 animals per group, necropsy at day 8 or 22): control (0 mg), low-dose (0.06 mg), mid-dose (0.25 mg), and high-dose (1.0 mg), corresponding to 0X, \sim 2.5X, \sim 10X, and \sim 42X, respectively, of a human nusinersen dose (12 mg) after scaling for rat vs. human CSF compartmental volumes. Animals in the 0 mg and 0.06 mg groups exhibited no adverse effects for the entire 22 day follow-up period based on either clinical observations or detailed functional neurologic assessments. Half the animals in the 0.25 mg group and most of the animals in the 1.0 mg group demonstrated transient hindlimb weakness and gait abnormalities, lasting up to 24 hours after each dose. Transient (\sim 24 hours) hindlimb neurologic deficits were also reported in cynomolgus monkeys receiving intrathecal bolus administration of nusinersen at \geq 4 mg, which corresponds to \geq 0.1 mg in rats after compartmental scaling (see CDER Pharmacology Review, Application Number 209531Orig1s000; Section 2.3.4, and April 2017 EMA nusinersen assessment report), suggesting similarity in safety profiles. No other adverse effects were noted in any animals in the four groups, in hematology, clinical chemistry, or neuropathological assessments at day 8 or day 22. (Neuropathological analysis included tissue examination of the injection site, lumbar and cervical spinal cord, brain, and meninges, but not dorsal root ganglia; see below.)

Double-dose tolerability: Rats were given two consecutive (7 days apart) intrathecal injections of milasen diluted in 50 μ l artificial CSF per each injection. Animals were divided into three groups by dose level per injection: control (0 mg, 25 animals), mid-dose (0.25 mg, 20 animals), and high-dose (1.0 mg, 25

animals). Some animals in the 0.25 mg group exhibited neuropathologic evidence of DRG toxicity (minimal to mild neurodegenerative changes seen in 5/10 animals sacrificed on day 22), but exhibited no behavioral or neurologic consequences (observed out to day 70). Animals in the 1.0 mg group developed delayed hindlimb gait abnormalities at day 34 post initial injection. This behavioral abnormality was accompanied by minimal to mild neuropathological evidence of dorsal root ganglion (DRG) toxicity. Hindlimb gait abnormalities began to improve by day 53 and disappeared by day 66 (**Fig. S13**). Minimal to mild DRG degenerative changes were seen upon microscopic evaluation at the completion of the follow-up period (day 141).

Multi-dose tolerability: Rats were given seven (day 1, 7, 70, 84, 98, 112, 126) intrathecal injections of milasen diluted in 50 μ l (first two doses) or 33 μ l (subsequent five doses) artificial CSF. Animals were divided into two groups by dose level per injection: control (0 mg, 9 animals) and mid-dose (0.25 mg, 9 animals). As before, some animals exhibited only transient (<24 hours) hindlimb gait abnormalities in response to each dose but after the seventh injection (day 126) these hindlimb gait abnormalities became persistent. Histopathological evaluation showed evidence of minimal to mild DRG degeneration at day 103 (1 week after the fifth injection) and 141 (2 weeks after the seventh injection).

Our findings of hindlimb gait and sensory changes induced by high doses of milasen in these experiments provided translatable and readily monitorable indicators that were used to guide safety monitoring in our clinical protocol design.

Seizure characteristics

The seizures were stereotyped, starting with a generalized spike and wave correlating clinically with a myoclonic seizure (corroborated by EMG electrodes), followed by rhythmic theta activity that evolved in the bilateral temporal regions, during which the patient experienced the unusual laughter. The semiology did not change over time but the intensity of the laughter and the repetitive hand movement decreased. On

one occasion during the EEG on day 118, a cluster of pure myoclonic seizures was recorded which was not seen later on EEGs or clinically by family. Her EEG background did not change throughout the four performed EEGs. It consisted of continuous generalized slowing with no well-formed wakefulness or sleep features, and frequent multifocal sharp waves and generalized spike and wave discharges.

Natural history

With only ~70 patients with *CLN7* disease described in the literature, formal natural history studies have yet to be published. Still, *CLN7* and other Batten diseases are well known to be devastating and invariably progressive. In the largest published case series of 25 patients with *CLN7* disease, the mean age of onset was 3.3 years, and seven patients died at a mean age of 11.5 years.¹⁵ Continued monitoring is ongoing, but this is the first case where apparent stability of the disease over eleven months has been reported.

Biomarker

The causative gene for *CLN7* Batten disease, *MFSD8*, was only identified in 2007,¹⁶ and there are no known biomarkers. *MFSD8/CLN7* encodes a multi-pass transmembrane domain protein. There are as of yet no specific antibodies available, and while it is presumed to act as a lysosomal transporter protein, its substrate(s) remains to be identified.¹⁶

Patient eligibility considerations

Contemplation of our approach, at this point, should be restricted to patients with diseases that are exceptionally serious or life-threatening as it still bears significant risks. In addition, it should be noted that only a minority of patients are likely to have amenable mutations via this specific strategy. Based on our own unpublished observations, this may be as low as ~2% of patients in WES (whole exome sequencing)-based rare disease registries and up to ~15% based on WGS-based registries (reflecting the fact that many amenable mutations are being missed by exon-based sequencing approaches). Additional factors were whether or not treatment may be reasonably expected to correct disease trajectory, the

availability of alternative disease-modifying treatment options, the patient's current functional status, the treatment efficacy in patient-derived cells, the efficacy and safety profile of the proposed modality and administration route, the future option to stop treatment in case of futility or toxicity, and the ability of the family to appreciate these potential benefits and risks of participation. In our case, each of these factors was evaluated by the research team as well as our Institutional Review Board, Ethics Committee, Gene and Cellular Therapy Committee, and Experimental Therapeutics and Interventional Trials Center, and we suggest that similar considerations (**Table S6**) should inform future cases where novel personalized therapies may be contemplated. These patient eligibility considerations are conservative, and of course could be modified depending on future technological improvements and validations. For example, it has been previously reported that conjugation of ASOs to various moieties can dramatically increase delivery to specific organs (*e.g.*, liver for GalNAc-conjugated ASOs,¹⁷ or pancreatic islet cells for eGLP1¹⁸); if these conjugation technologies are proven safe and effective, criteria could be expanded to include diseases these tissues as well.

Future challenges in scaling

If this approach to therapy is to scale, many systemic and infrastructural issues will have to be addressed: (1) addressing gaps in regulatory guidance regarding appropriate standards for manufacturing and safety testing, given different risk-benefit calculations for individualized drugs for fatal, life-threatening, and orphan conditions, (2) standardizing and streamlining the development process, (3) establishing scalable manufacturing and toxicology infrastructure, (4) defining reimbursement strategies, (5) wrestling with the underlying issue of jurisdiction: what constitutes the practice of medicine vs. what constitutes commercial development for drugs to market, (6) managing institutional risk and liability. Many of these issues directly or indirectly impact cost. We believe that innovations in technology and regulation will make it possible to scale this process to benefit a large number of patients without putting an excessive financial burden on families or the system.

SUPPLEMENTARY FIGURES S1–S18

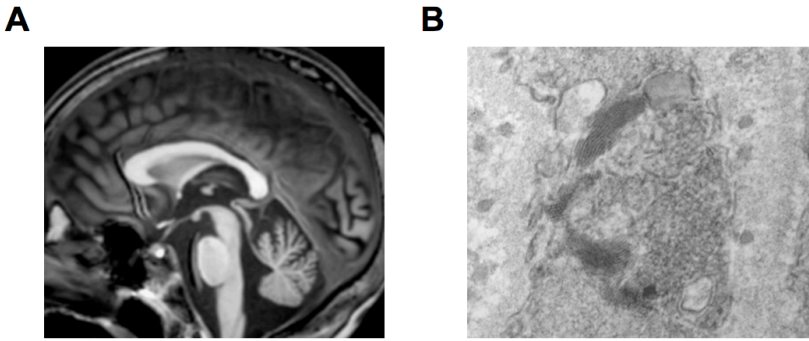


Figure S1. Initial clinical diagnosis. (A) Brain atrophy observed from MRI of the patient brain at the initial presentation. (B) Fingerprint pattern observed from electron microscopy on skin biopsy, which is characteristic of Batten disease.

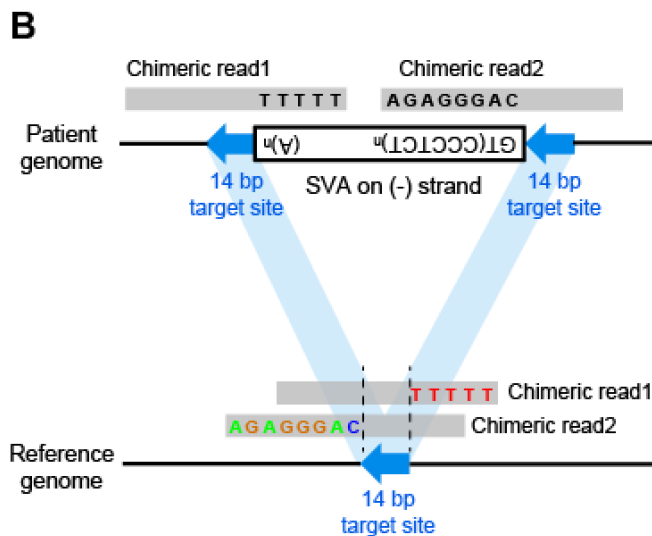
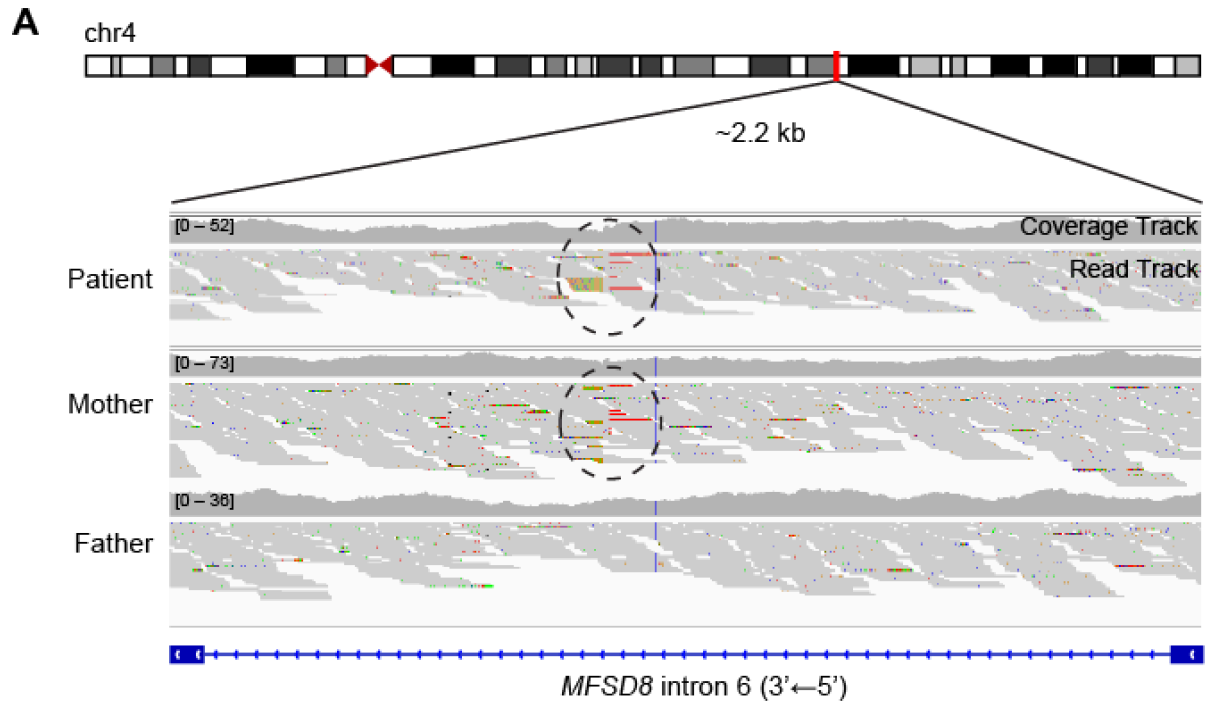


Figure S2. Observation of the SVA insertion in patient's genome. (A) A screenshot of Integrative Genomics Viewer (IGV), showing WGS read alignments of the patient trio in the ~2.2 kb region encompassing *MFSD8/CLN7* intron 6 (chr4:128,861,040-128,863,258, hg19). Indicated with dotted circles are the clusters of read alignments that provide supports for an SVA retrotransposon insertion. (B) A schematic illustrating how chimeric reads that originated from the patient's genome would align on the reference genome. As the SVA transposon is inserted in the minus strand of the patient's genome (*i.e.*, the sense strand of *MFSD8/CLN7*), WGS reads from the boundaries of the insertion will only partially align to the reference genome with a soft-clipped overhang of either polyT or hexameric repeat sequences.

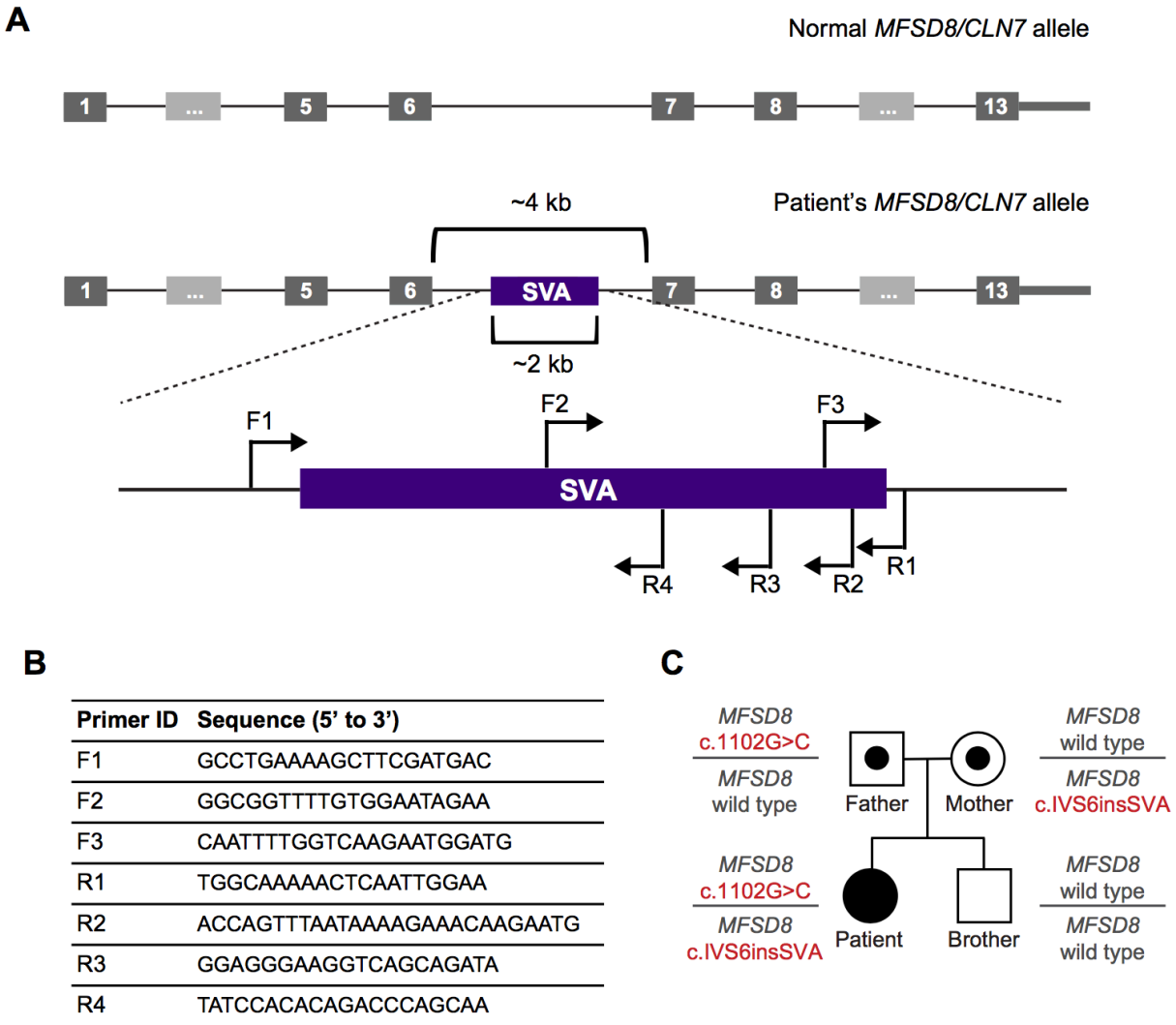


Figure S3. Confirmation of the SVA insertion. (A) The full sequence of the SVA retrotransposon insertion in patient's genome, revealed by chromosomal walking and Sanger sequencing. The location and direction of Sanger sequencing primers are indicated. (B) Sequences of Sanger sequencing primers. (C) The mutational statuses of patient's family members, confirmed by an independent CLIA-based clinical sequencing provider.

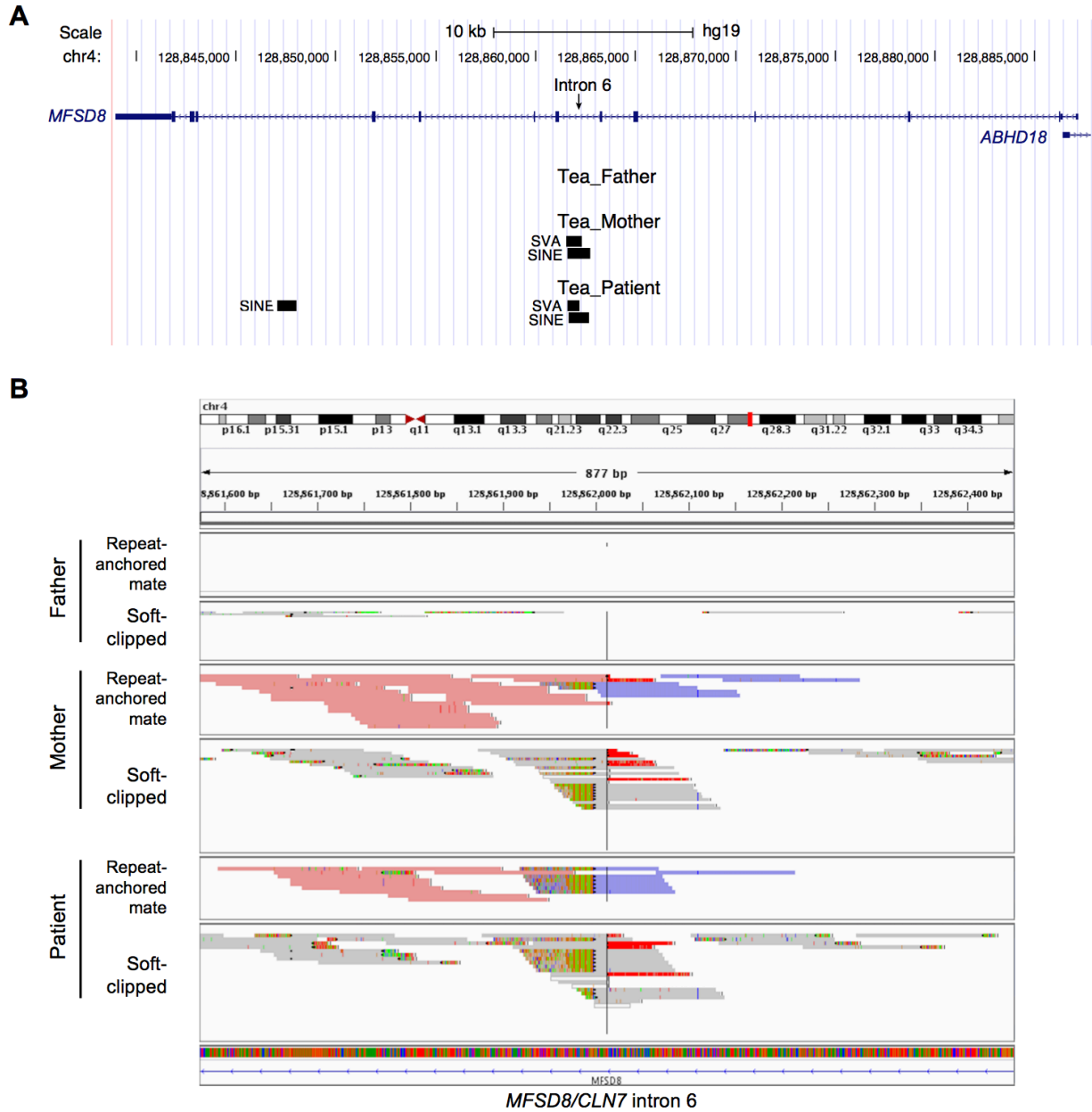


Figure S4. Automated retrotransposon detection by the Tea algorithm. (A) Transposable elements in *MFSD8/CLN7*, predicted by the Tea algorithm on the WGS data of the patient trio. The SVA (SINE-VNTR-*Alu*) insertions are often predicted as SINE as well, due to the homology between the two types of insertions. (B) IGV visualization of selected WGS reads that support the transposable element insertions in *MFSD8/CLN7* intron 6 in patient's and mother's genome. Repeat-anchored mate tracks display each mate of paired-end reads whose conjugate mate is mapping to the foreign sequence of the insert. Red and blue colors indicate that the mate is mapped in the forward and reverse orientation, respectively. Soft-clipped track displays reads that are partially aligned.

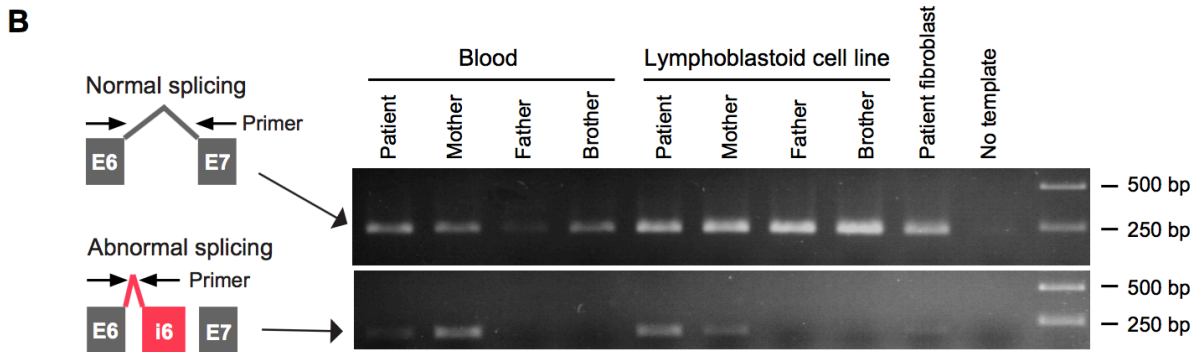
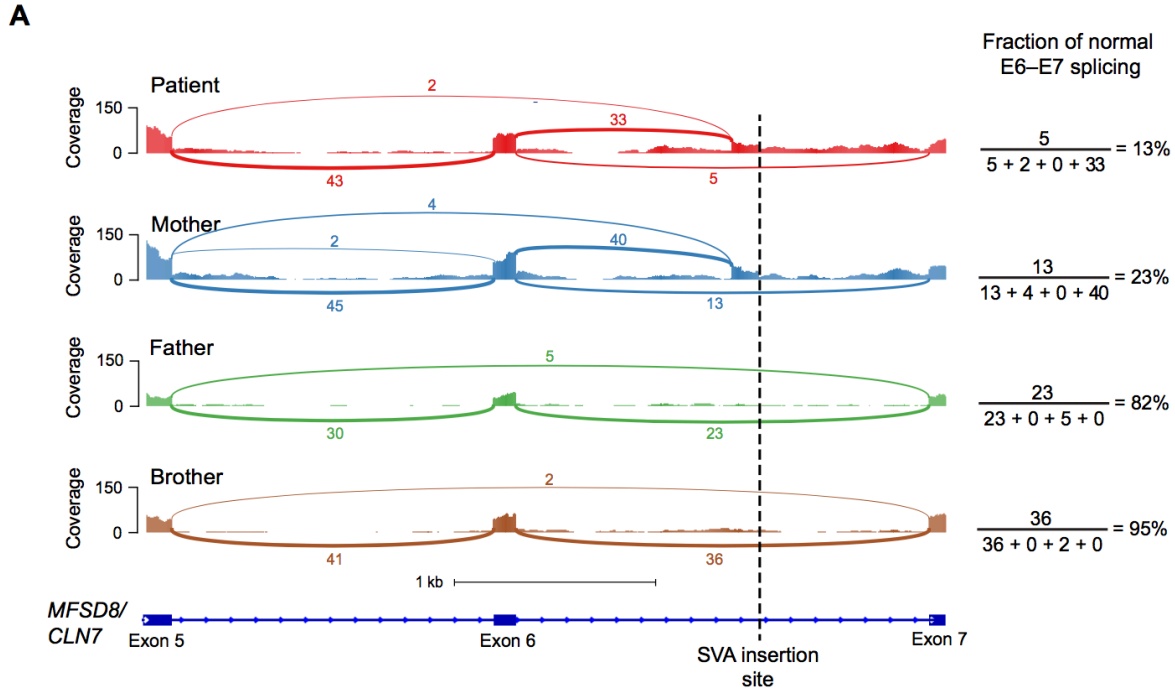


Figure S5. SVA-induced exon trapping, identified by RNA-seq and RT-PCR analyses. (A) Exon trapping and premature translational termination of *MFSD8/CLN7* by the SVA insertion in the patient and the mother, revealed by RNA-seq analysis of lymphoblastoid cell lines from the patient's four family members, analyzed as for **Figure 2C**. **(B)** RT-PCR confirmation of the exon trapping by the SVA insertion.

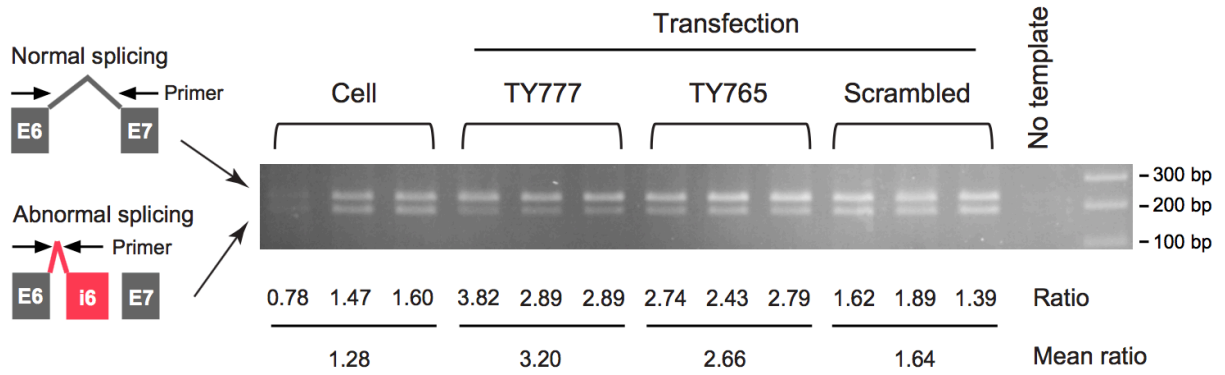


Figure S6. Multiplex RT-PCR assay for the screening of ASOs that rescue exon trapping. An example multiplex PCR followed by gel electrophoresis, used to obtain the results in **Figure 2B**. “Ratio” indicates the ratio of the normal exon 6 to exon 7 (E6–E7) splicing (upper band) to the abnormal exon 6 to intron 6 (E6–i6) splicing (lower band), measured by gel band intensity quantification.

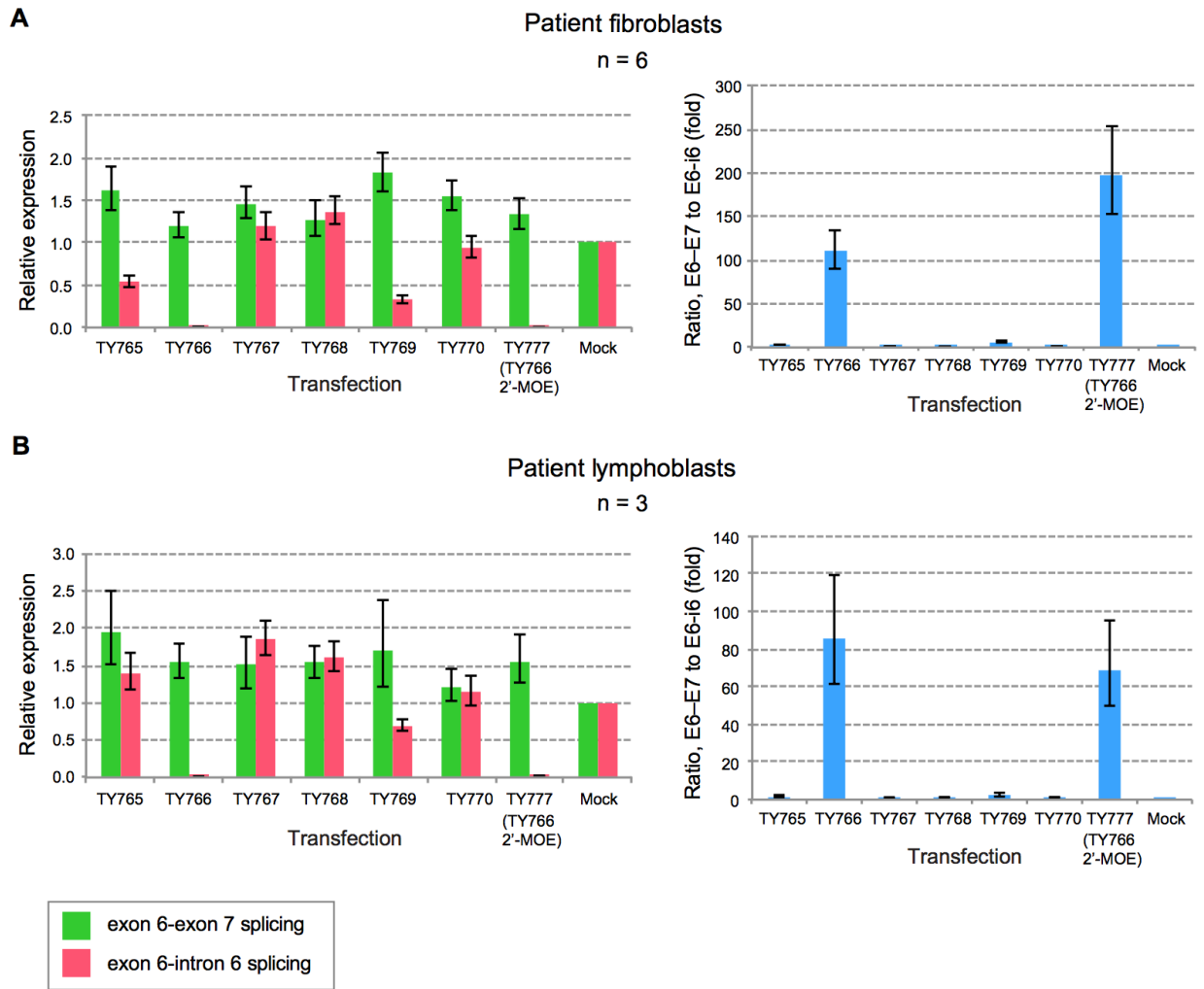


Figure S7. Confirmation of the efficacy of milasen/TY777 by blinded experiments conducted by an independent laboratory. (A) Patient cell lines and oligonucleotide reagents were provided to the BCH TransLab, a translational and clinical research core at Boston Children's Hospital, for blinded replication. ASOs were transfected into patient's fibroblasts at 100 nM final concentration. Isoform-specific transcript levels were measured by multiplex qRT-PCR (Table S2). Milasen/TY777 has the same sequence as TY766, but is phosphorothioate, 2'-MOE-modified as opposed to phosphorothioate, 2'-OME-modified. Error bars represent 95% confidence interval of the means. (B) Same as panel A, but for patient's lymphoblasts.

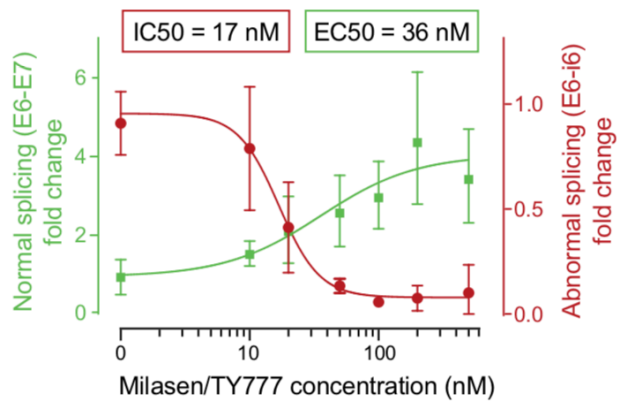


Figure S8. Dose-response relationship. qRT-PCR was used to quantify isoform-specific expression (Table S2). Error bars, standard deviations of triplicates.

A**Genomic matches of milasen/TY777 subsequences**

Length (nt)	Number of possible subsequences	Number of off-target hits	Off-target locus (hg19)	Gene annotation (RefSeq)		
				Gene	Strand	Region
22	1	0	-	-	-	-
21	2	0	-	-	-	-
20	3	0	-	-	-	-
19	4	0	-	-	-	-
18	5	0	-	-	-	-
17	6	0	-	-	-	-
16	7	7	chr8:133920812-133920827	<i>TG</i>	sense	intron (>225 bp away from junction)
			chr2:31419168-31419183	<i>CAPN14</i>	antisense	intron (>930 bp away from junction)
			chr7:11557766-11557781	<i>THSD7A</i>	antisense	intron (>23 kb away from junction)
			chr14:44523991-44524006	-	-	-
			chr21:39879432-39879447	<i>ERG</i>	sense	intron (>33 kb away from junction)
			chr5:32260334-32260349	<i>MTMR12</i>	antisense	intron (>2.8 kb away from junction)
			chr2:65886796-65886811	-	-	-

B**Genomic matches of nusinersen subsequences**

Length (nt)	Number of possible subsequences	Number of off-target hits	Off-target locus (hg19)	Gene annotation (RefSeq)		
				Gene	Strand	Region
18	1	0	-	-	-	-
17	2	3	chr2:151151798-151151814	-	-	-
			chr6:137801026-137801042	-	-	-
			chr12:129939692-129939708	<i>TMEM132D</i>	sense	intron (>75 kb away from junction)
16	3	7	chr13:30033807-30033822	<i>MTUS2</i>	antisense	intron (>19 kb away from junction)
			chr3:82606750-82606765	-	-	-
			chr15:32439151-32439166	<i>CHRNA7</i>	sense	intron (>6.9 kb away from junction)
			chr20:9638297-9638312	<i>PAK5</i>	sense	intron (>13 kb away from junction)
			chr7:125728305-125728320	-	-	-
			chr7:141917297-141917312	<i>MGAM2</i>	sense	intron (>800 bp away from junction)
			chr3:110103460-110103475	-	-	-

Figure S9. Genomic off-target footprints of milasen/TY777, compared to those of nusinersen. (A) All possible subsequences of a given length were taken from the milasen/TY777 sequence and aligned to the reference human genome. The number and identity of the off-target matches are shown. If the off-target locus is in an intron, the distance from the closest splice junction is indicated. **(B)** same as in panel A, but for nusinersen. Also see Supplementary Text.

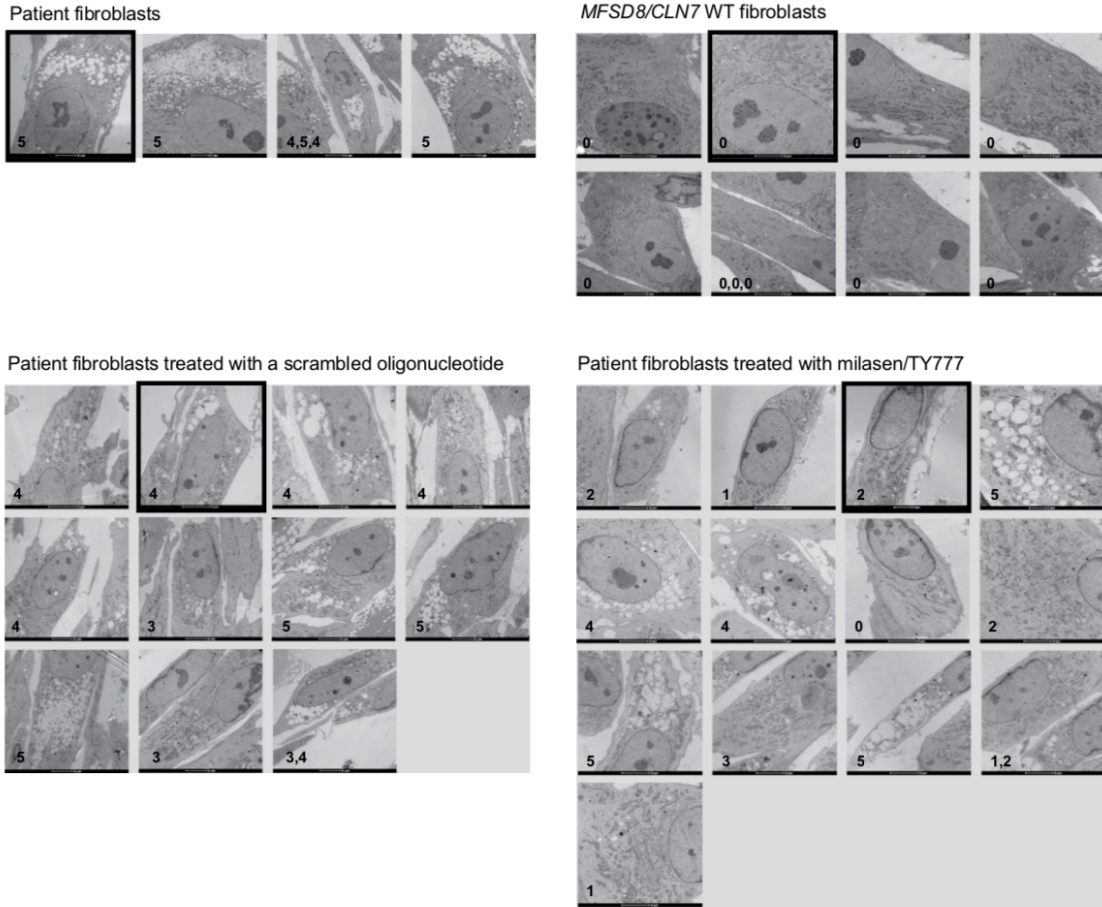
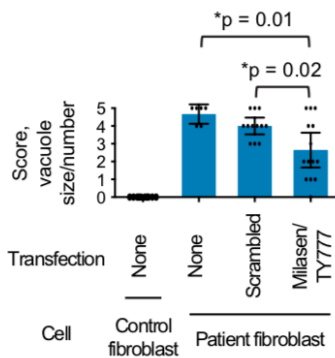
A**B**

Figure S10. Electron microscopy of normal and patient fibroblasts for visualization of accumulated vacuoles. (A) Scores in the bottom left corner of each image indicate intracellular vacuole level ranging from 0 to 5 (0 and 5 representing the lowest and highest accumulation, respectively). The scoring was performed by manual inspection in a blinded manner. Some images showed more than one cell, in which case, scoring was done for each cell. The length of the white bar at the bottom of each image corresponds to 5 μm. The representative images for each group, used in **Figure 2D**, are indicated by black squares. (B) Intracellular vacuole numbers and sizes, quantified as scores of 0 to 5 from the electron microscopy images in panel A. Error bars, 95% confidence interval of the means. *p < 0.05, two-sided t test.

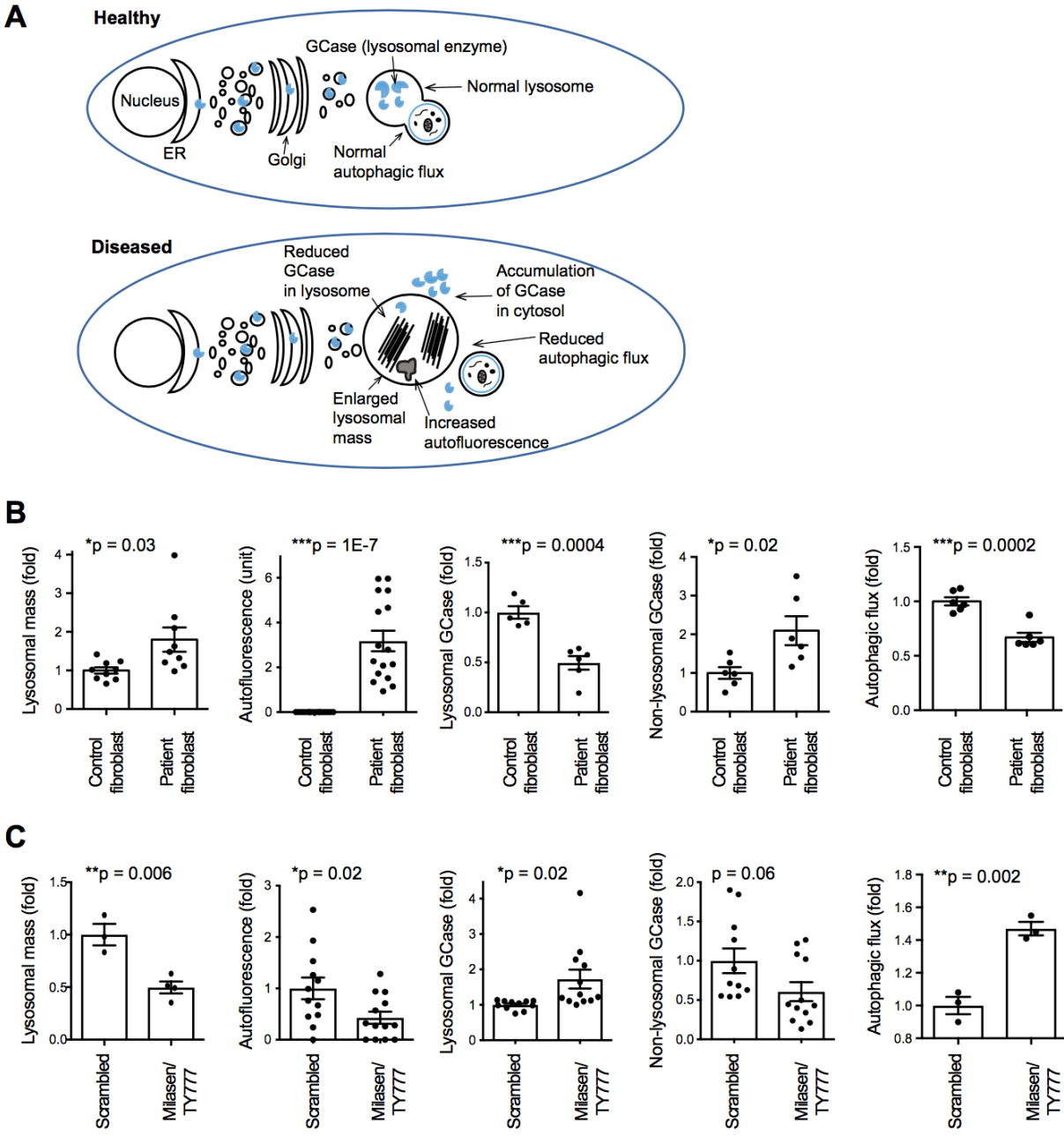


Figure S11. Rescue of lysosomal function by milasen/TY777. (A) Readouts of lysosomal function assays, reflecting healthy (top) and diseased (bottom) cellular states. (B) Differences in lysosomal function between patient fibroblasts and control fibroblasts (*MFSD8/CLN7* wild type; BJ cell line) (both untreated). *p < 0.05, **p < 0.005, ***p < 0.0005, two-sided t test. (C) Differences in lysosomal function between the patient fibroblasts treated with a scrambled oligonucleotide and milasen/TY777. Also see Supplementary Text.

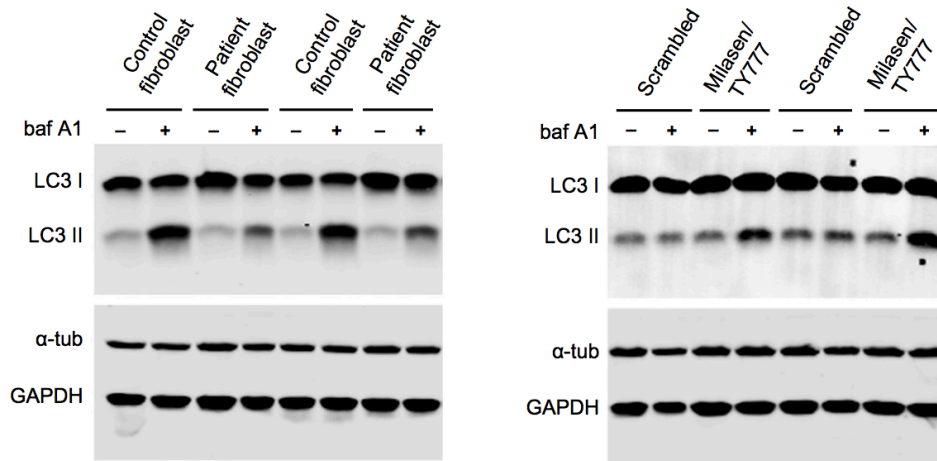
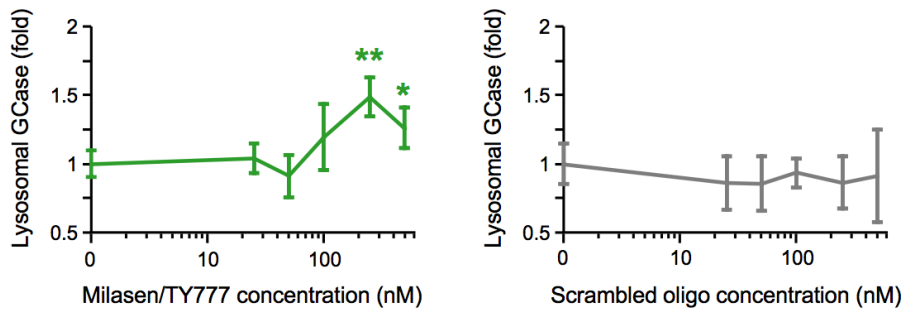
A**B**

Figure S12. Rescue of autophagic flux and dose-dependence rescue of lysosomal enzyme activity by milasen/TY777. (A) Autophagic flux analysis. Western blot results that were used to draw the bar graphs on the far right side of **Figures S11B-C**. Autophagic flux is calculated by measuring the change in LC3-II upon baf A1 treatment. LC3-II is the lipidated form of LC3 and is an indication of autophagosome number. As baf A1 inhibits autophagosome-lysosome fusion, the increase in LC3-II upon baf A1 treatment indicates autophagic flux. The results show that autophagic flux in patient fibroblasts is weaker than in control fibroblasts (*MFSD8/CLN7* wild type; BJ cell line), and it is restored by milasen treatment to near control level. (B) Dose-dependent restoration of lysosomal GCase activity by milasen. $n = 5$ at each dose. Error bars, 95% confidence interval. $**p < 0.005$ and $*p < 0.05$, two-sided t test (compared to no transfection control).

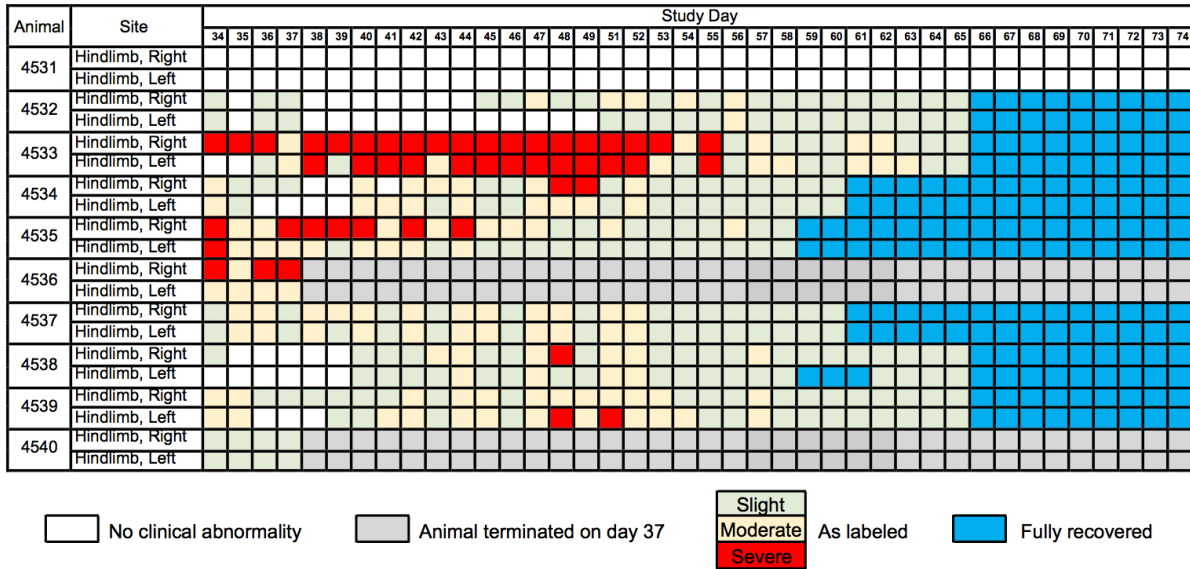


Figure S13. Delayed onset and natural resolution of hindlimb weakness in repeat, 1.0 mg-dosed rats. Incidence and severity of limited usage of the hindlimbs in rats receiving 1.0 mg x 2 intrathecal milasen. Female Sprague-Dawley rats received 1.0 mg of intrathecal milasen via spinal catheter on days 1 and 8. Clinical observations from days 34-74 are shown, demonstrating hindlimb gait abnormalities in 10/10 rats from this dosing group, lasting approximately 30 days, with full resolution. This effect was not observed in rats in the next lower dose exposure group (0.25 mg on days 1 and 8, data not shown). Also see Supplementary Text.

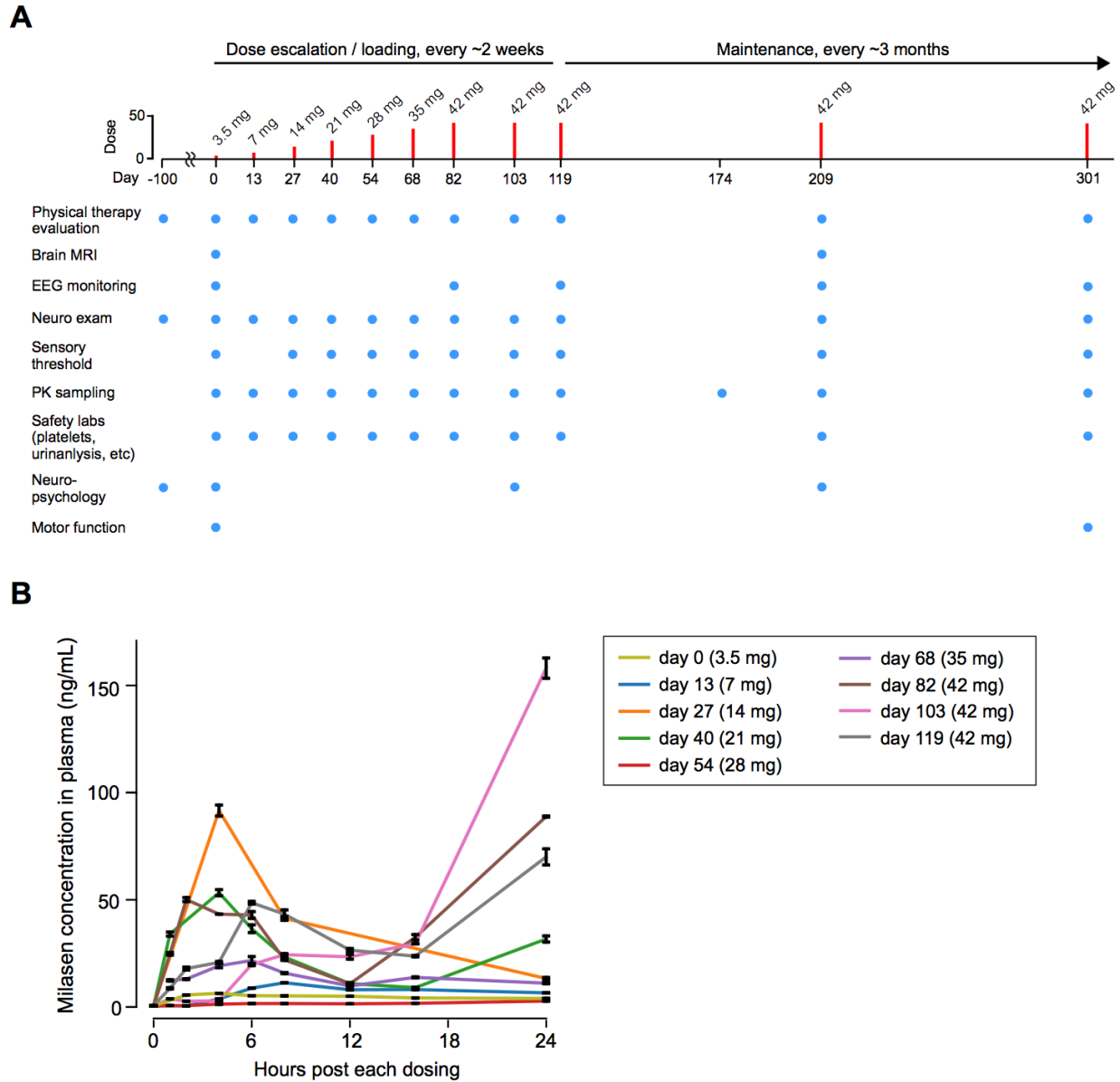


Figure S14. Clinical protocol and plasma pharmacokinetics. (A) Clinical protocol. Also see Supplementary Text. (B) Milasen concentration in plasma at immediately prior to each administration or at multiple time points within the 24 hours after each administration. Data obtained at day-209 and -301 injections were not shown as plasma pharmacokinetics sampling was done only for 0 (pre-dose), 1, and 2 hour time points for those injections. Error bars indicate the min and max values of duplicate measurements. The lower limit of quantification was 0.5 ng/mL. Notably, plasma drug levels following each dose demonstrated a bimodal pattern. Drug concentrations peaked at ~4 hours and ~24 hours in the systemic circulation, suggesting acute and delayed leak of the drug to the systemic circulation. However, the systemic exposure of the drug is not sustained, as plasma drug levels prior to each dose (trough levels) were below the lower limit of quantification (0.5 ng/mL) throughout the study.

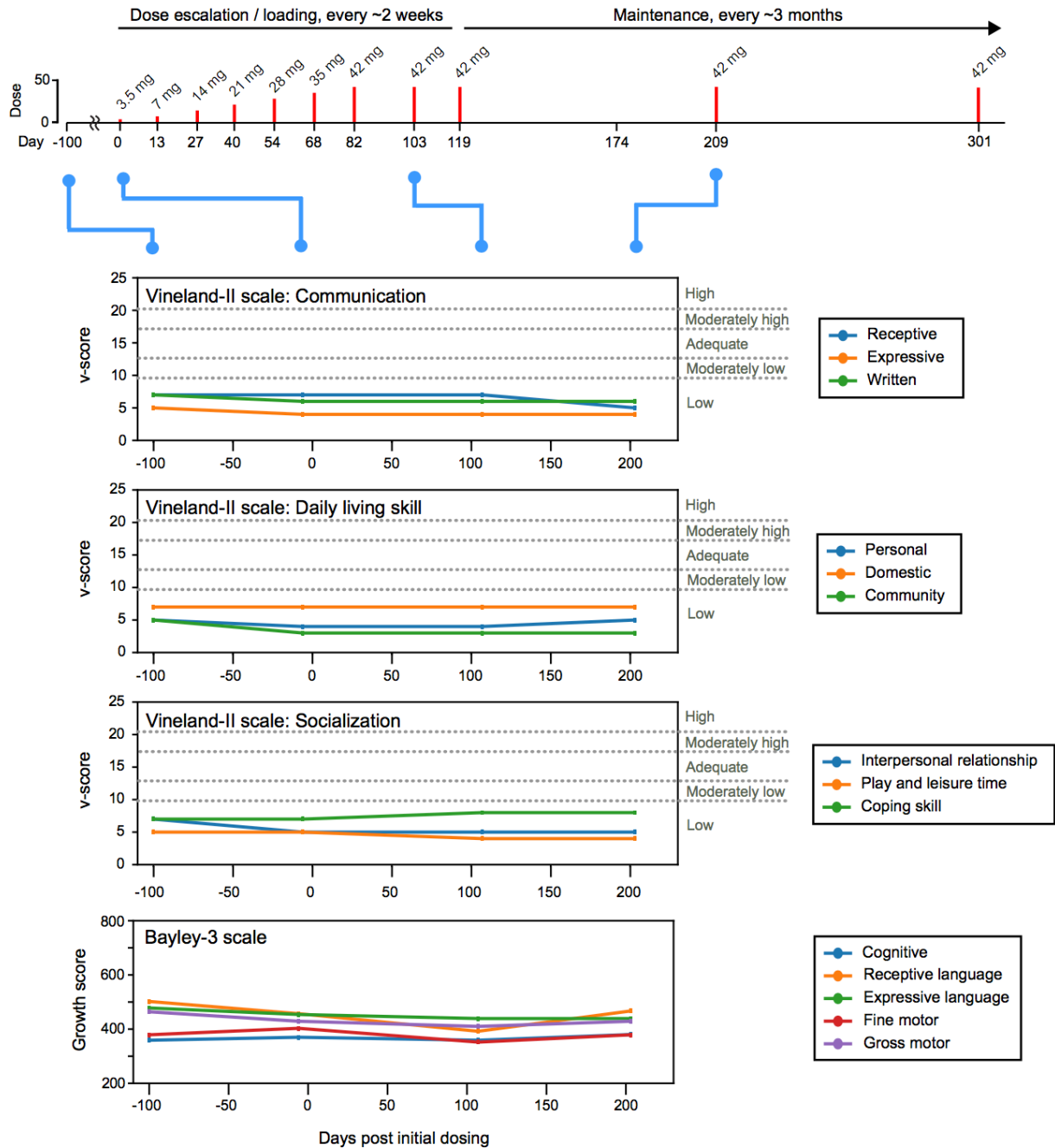


Figure S15. Neuropsychological assessments. Neuropsychological tests based on Vineland-II and Bayley-3 scales were performed at the indicated time-points before and after drug administration. Bayley-3 assessments at these time-points were more difficult to interpret as they proved more subject to circumstances specific to the day of administration (unlike the Vineland-II, which is based on parent report), not necessarily representative of her day-to-day functioning. For instance, she was extremely fatigued on day 107 because of disrupted sleep from two days of inpatient admission immediately prior. On the whole, there was no consistent pattern of decline or improvement in Bayley-3 subscores between days -6 and day 203. Also see **Table S4** and **S5** for the full set of scores.

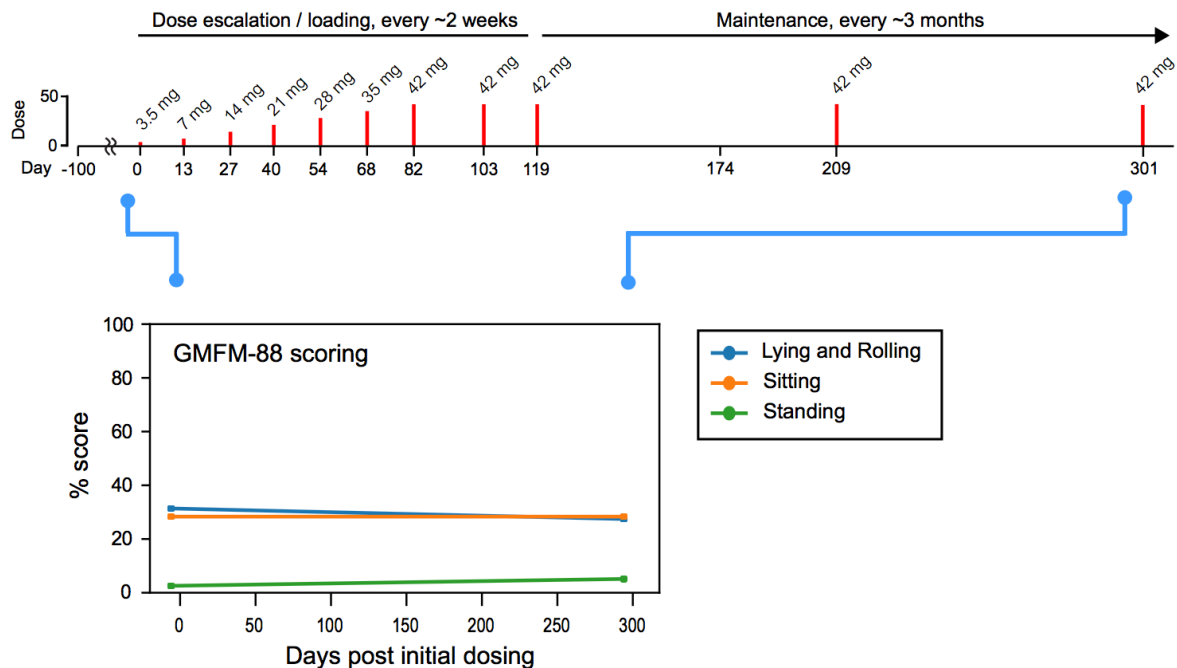


Figure S16. Gross motor function. The Gross Motor Function Measure-88 (GMFM-88) was administered during the screening visit before the initial dose (6 days prior to the initial dosing), and again on 294 days post the initial dosing. The graph includes total raw scores – normalized to percentage – for the Lying and Rolling, Sitting and Standing Domains. The subject scored 0 on the Crawling and Kneeling and Walking, and Running and Jumping Domains.

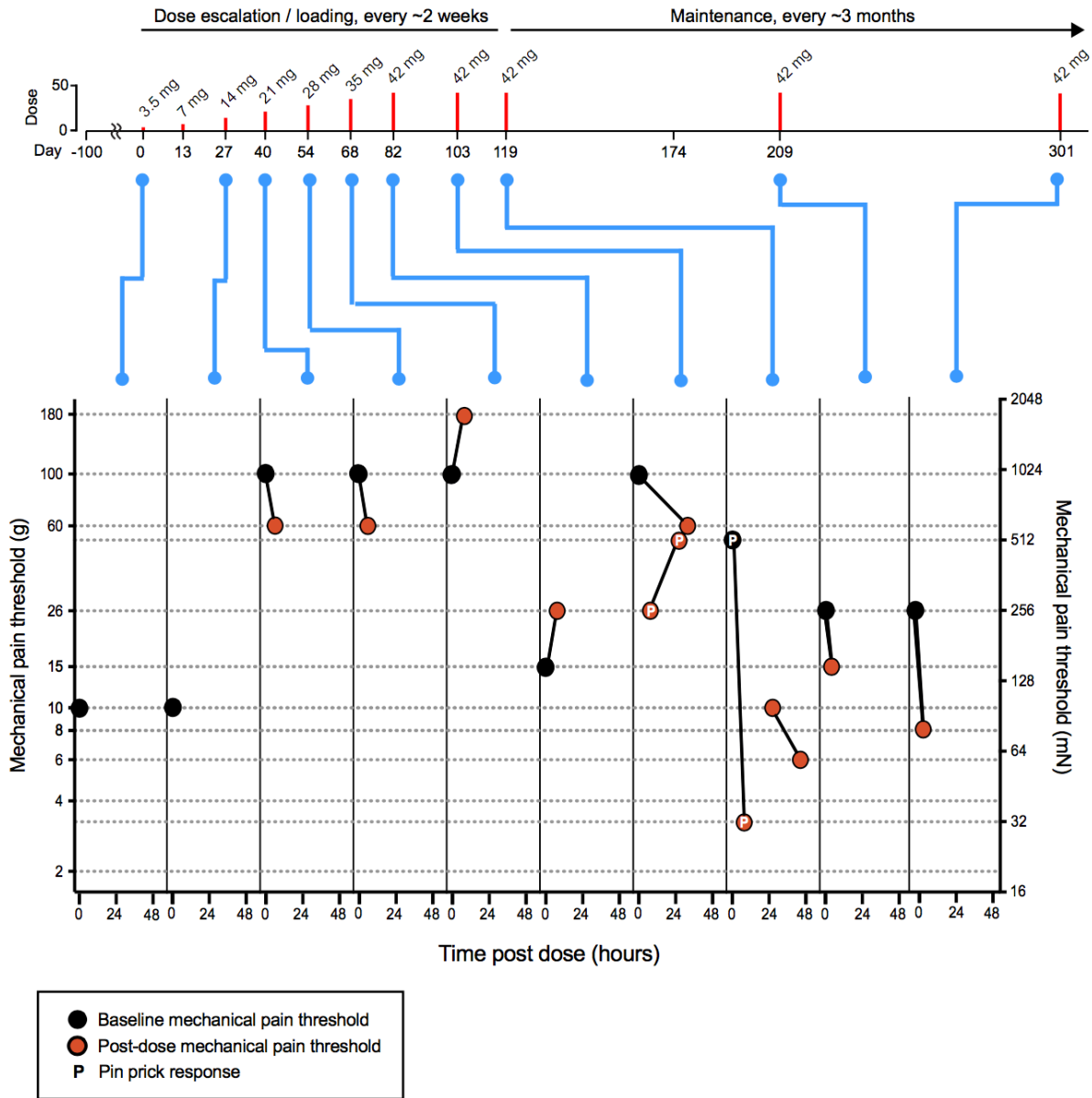


Figure S17. Sensory threshold. Mechanical pain threshold was measured at the indicated time points after each drug administration. The threshold is defined as the vFh (g-force) required to evoke a response. Y axis is in log₂ scale, but the ticks were labeled with values in linear scale. The pin prick method was used when no response was present to the von Frey hair punctate simulation. Three consecutive tests were performed with the inter-stimulus interval between the stimuli being ~2 seconds. The median of the three measurements is indicated for each time point.

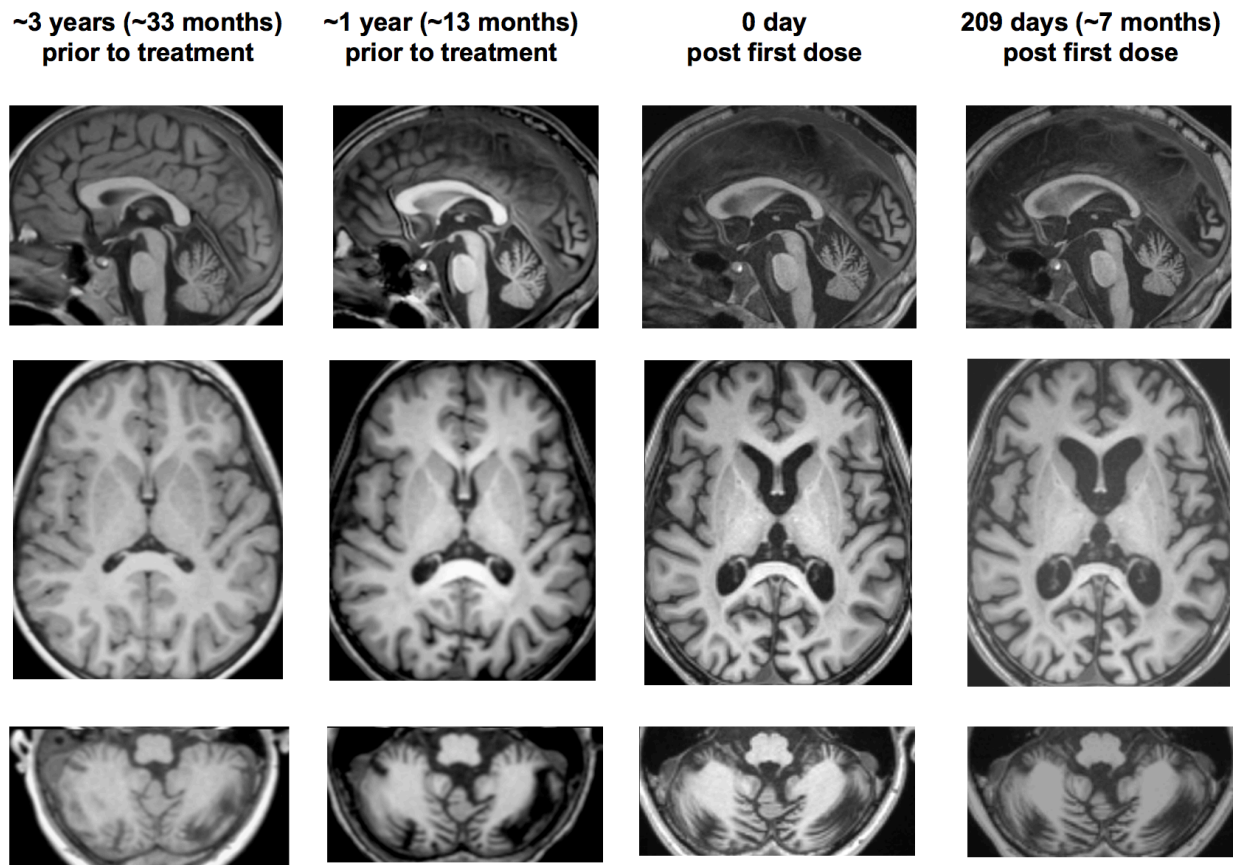


Figure S18. Change in cerebral and cerebellar morphology, visualized by brain MRI. Brain MRI showed significant cerebral and cerebellar volume loss in the three year period prior to treatment. Despite the positive clinical trends noted in seizure trends and neuropsychological assessments, MRI at ~7 months (day 209) continued to show modest (cerebral greater than cerebellar) volume loss compared to trial onset (day 0). This is however consistent with a prior large animal study of gene therapy for the related *CLN5* Batten subtype, in which animals treated after symptom onset continue to exhibit brain volume loss for over 20 months, despite treatment substantially slowing functional deterioration, showing that continued volume loss can be driven by disease cascades set in motion prior to therapy.¹⁹

SUPPLEMENTARY TABLES S1–S6

Table S1. ASO sequences and chemistry

ID	Sequence	Chemistry
TY765	AGCUUUUCAGGCUUACAUUUACUCAUCU	2'-OMe
TY766	AAUGUUAGUGCUUGUUGAGGGC	2'-OMe
TY767	CUAGCAUACAGUAAGCACACA	2'-OMe
TY768	CUUUAAAUGCUUUUAAGGUGGUA	2'-OMe
TY769	CAGGCUUACAUUUACUCAUCU	2'-OMe
TY770	GUCAUCGAAGCUUUUCAGG	2'-OMe
TY777	AATGTTAGTGCTTGTGAGGGC	2'-MOE, 5Me-C
Scrambled	CGCGACUAUACGCGCAAUAUGC	2'-OMe

*All ASOs have phosphorothioate-modified backbone at every position

Table S2. Primer and probe sequences for isoform-specific qPCR

Amplicon name	Sequence	Type	Amplicon size (bp)
MFSD8_E6-i6	5'-AGCATGTGTCAAGCATTAGGT	forward primer	101
	5'-AGTGCTTGTGAGGGCTTATT	reverse primer	
	5'-AGGTCCAGATGAGTAAATGTAAGCCTGA	probe	
MFSD8_E6-E7	5'-ACATAAGCATGTGTCAAGCATTAG	forward primer	150
	5'-CCAGGAAGGCGCTAAGTAAA	reverse primer	
	5'-AGGTGTGACATGGGATGTGATTAAGTGC	probe	
GAPDH	5'-GGTGTGAACCATGAGAAGTATGA	forward primer	123
	5'-GAGTCCTTCCACGATACCAAAG	reverse primer	
	5'-AGATCATCAGCAATGCCTCCTGCA	probe	

Table S3. Adverse events. Adverse events (AEs) were assessed according to the NCI’s CTCAE version 4.0. Grades can range from 1 to 5, with 3, 4, and 5 indicating severe but not life-threatening, life-threatening, and death, respectively. All AEs of grade 2 and higher are listed. There were no serious AEs during the course of the study. No clinically significant adverse changes in vital signs, neurologic or physical examinations, clinical laboratory tests, or CSF profiles were observed. Adverse events and toxicities were captured both by planned laboratory studies, as well as by patient/family reporting.

Adverse event	Grade	Attribution to milasen	Attribution to procedure	Expectedness	Number of times occurred
Hypertension	1	Possibly related	Possibly related	Expected for procedure	1
Neutrophil count decrease	2	Unrelated	Unrelated	Expected for disease	3
Pain	2	Unrelated	Probably related	Expected for procedure	1
CSF pleocytosis	1	Possibly related	Possibly related	Possibly	4
Protein in CSF	1	Possibly related	Possibly related	Possibly	Ongoing
Cytokines increased	2	Unrelated	Unrelated	Expected for disease	2
Laryngospasm	2	Unrelated	Related	Expected for procedure	2
Hypotension	2	Unrelated	Related	Expected for procedure	9
Anemia	2	Unrelated	Unrelated	Expected for disease	1
Intermittent fatigue	2	Unrelated	Unrelated	Expected for hospitalization	Ongoing
Blood bicarbonate decrease	2	Unrelated	Unrelated	Expected for hospitalization	1
Intermittent insomnia	2	Unrelated	Related	Possibly	Ongoing
Toxic synovitis	2	Unrelated	Unrelated	Unexpected	1
Myositis	2	Unrelated	Unrelated	Unexpected	1
Scoliosis	2	Unrelated	Unrelated	Expected for disease	Ongoing

Table S4. Neuropsychology assessment: Vineland-II scores. v-scores range from 0 to 25. Also see Figure S15.

Domain	Day -100 (10/23/2017)		Day -6 (1/25/2018)		Day 107 (5/18/2018)		Day 203 (8/22/2018)	
	Raw	v-score	Raw	v-score	Raw	v-score	Raw	v-score
<i>Communication</i>								
Receptive	16	7	13	7	13	7	10	5
Expressive	17	5	10	4	10	4	12	4
Written	0	7	0	6	0	6	0	6
<i>Daily Living Skills</i>								
Personal	12	5	8	4	5	4	6	5
Domestic	0	7	0	7	0	7	1	7
Community	4	5	0	3	0	3	0	3
<i>Socialization</i>								
Interpersonal relationships	23	7	14	5	13	5	15	5
Play and leisure Time	7	5	4	5	4	4	3	4
Coping skills	0	7	2	7	6	8	8	8
<i>Motor Skills</i>								
Gross	11	-	10	-	16	-	6	-
Fine	3	-	6	-	5	-	4	-

Table S5. Neuropsychology assessment: Bayley-3 scores. Growth scores range from 200 to 800. Also see **Figure S15**.

Domain	Day -100 (10/23/2017)		Day -6 (1/25/2018)		Day 107 (5/18/2018)		Day 203 (8/22/2018)	
	Raw	Growth score	Raw	Growth score	Raw	Growth score	Raw	Growth score
Cognitive	10	359	12	370	10	359	14	380
Receptive language	15	502	11	457	7	392	12	467
Expressive language	14	478	11	454	9	439	9	439
Fine motor	10	379	13	403	6	352	10	379
Gross motor	32	464	23	429	18	410	23	429

Table S6. Patient eligibility considerations. Also see Supplementary Text.

	Consideration	Our patient
	Does the disease mainly affect CNS or eyes?	Yes (CNS)
	Is the disease life-threatening?	Yes (uniformly fatal)
	Is there an effective treatment available for the disease?	No
Disease	Does the disease have a defined genetic cause?	Yes (monogenic; loss of function of <i>MFSD8</i>)
	Is the disease course reversible or stoppable if the root genetic cause is addressed in a timely fashion?	Yes (arrest neurodegeneration)
	Are clinical endpoints available to monitor treatment efficacy?	Yes (seizure frequency and intensity)
	Is patient's causal pathogenic variant amenable to correction by ASO-mediated splice-switching approach?	Yes (SVA-induced splice trapping)
Patient	Is patient's functional status predicted to be good enough for treatment within the next one year?	Yes
	Do the patient or the family understand the potential risks and benefits of the treatment and wish to participate in the treatment?	Yes
Evidence	Was an ASO identified with demonstrated efficacy in patient-derived cells at the molecular and cellular phenotypic levels?	Yes (lysosomal function rescued in patient cells)

REFERENCES

1. Li, H. & Durbin, R. Fast and Accurate Short Read Alignment with Burrows-Wheeler Transform. *Bioinformatics* (2009).
2. McKenna, A. *et al.* The Genome Analysis Toolkit: a MapReduce framework for analyzing next-generation DNA sequencing data. *Genome Res.* **20**, 1297–303 (2010).
3. Lee, E. *et al.* Landscape of Somatic Retrotransposition in Human Cancers. *Science* (80-.). **337**, 967–971 (2012).
4. Fischbach, G. D. & Lord, C. The Simons Simplex Collection: A Resource for Identification of Autism Genetic Risk Factors. *Neuron* **68**, 192–195 (2010).
5. Bolger, A. M., Lohse, M. & Usadel, B. Trimmomatic: A flexible trimmer for Illumina sequence data. *Bioinformatics* **30**, 2114–2120 (2014).
6. Dobin, A. *et al.* STAR: ultrafast universal RNA-seq aligner. *Bioinformatics* **29**, 15–21 (2013).
7. Mazzulli, J. R., Zunke, F., Isacson, O., Studer, L. & Krainc, D. α -Synuclein-induced lysosomal dysfunction occurs through disruptions in protein trafficking in human midbrain synucleinopathy models. *Proc. Natl. Acad. Sci.* **113**, 1931–1936 (2016).
8. Bromage, P. R. Epidural Analgesia. *Philadelphia WB Saunders* **144**, (1978).
9. Breen, T. W., Shapiro, T., Glass, B., Foster-Payne, D. & Oriol, N. E. Epidural anesthesia for labor in an ambulatory patient. *Anesth. Analg.* **77**, 919–24 (1993).
10. Breschan, C. *et al.* A prospective study comparing the analgesic efficacy of levobupivacaine, ropivacaine and bupivacaine in pediatric patients undergoing caudal blockade. *Pediatr. Anesth.* **15**, 301–306 (2005).
11. IVANI, G. *et al.* Caudal anesthesia for minor pediatric surgery: a prospective randomized comparison of ropivacaine 0.2% vs levobupivacaine 0.2%. *Pediatr. Anesth.* **15**, 491–494 (2005).
12. Chin, J. J. *et al.* Novel mutations in CLN6 cause late-infantile neuronal ceroid lipofuscinosis without visual impairment in two unrelated patients. *Mol. Genet. Metab.* **126**, 188–195 (2019).
13. Platt, F. M., Boland, B. & van der Spoel, A. C. Lysosomal storage disorders: The cellular impact of lysosomal dysfunction. *J. Cell Biol.* **199**, 723–734 (2012).
14. Brandenstein, L., Schweizer, M., Sedlacik, J., Fiehler, J. & Storch, S. Lysosomal dysfunction and impaired autophagy in a novel mouse model deficient for the lysosomal membrane protein Cln7. *Hum. Mol. Genet.* **25**, 777–791 (2016).
15. Kousi, M. *et al.* Mutations in CLN7/MFSD8 are a common cause of variant late-infantile neuronal ceroid lipofuscinosis. *Brain* **132**, 810–819 (2009).
16. Siintola, E. *et al.* The Novel Neuronal Ceroid Lipofuscinosis Gene MFSD8 Encodes a Putative Lysosomal Transporter. *Am. J. Hum. Genet.* **81**, 136–146 (2007).
17. Huang, Y. Preclinical and Clinical Advances of GalNAc-Decorated Nucleic Acid Therapeutics. *Mol. Ther. - Nucleic Acids* **6**, 116–132 (2017).
18. Ämmälä, C. *et al.* Targeted delivery of antisense oligonucleotides to pancreatic β -cells. *Sci. Adv.* **4**, eaat3386 (2018).
19. Mitchell, N. L. *et al.* Longitudinal In Vivo Monitoring of the CNS Demonstrates the Efficacy of Gene Therapy in a Sheep Model of CLN5 Batten Disease. *Mol. Ther.* **26**, 1–13 (2018).